ORIGINAL PAPER

Electrodes modified with iron porphyrin and carbon nanotubes: application to CO_2 reduction and mechanism of synergistic electrocatalysis

Hua-Zhang Zhao · Ying-Yue Chang · Chuan Liu

Abstract Electrodes modified with iron porphyrin and carbon nanotubes (FeP–CNTs) were prepared and used for CO_2 electroreduction. The adsorption of iron porphyrin onto the multiwalled carbon nanotubes was characterized by scanning electron microscopy and ultraviolet and visible spectroscopy. The electrochemical properties of the modified electrodes for CO_2 reduction were investigated by cyclic voltammetry and CO_2 electrolysis. The FeP–CNT electrodes exhibited less negative cathode potential and higher reaction rate than the electrodes modified only with iron porphyrin or carbon nanotubes. A mechanism of the synergistic catalysis was proposed and studied by electrochemical impedance spectroscopy and electron paramagnetic resonance. The direct electron transfer between iron porphyrin and carbon nanotubes was examined. The current study shed light on the mechanism of synergistic catalysis between CNTs and metalloporphyrin, and the iron porphyrin–CNT-modified electrodes showed great potential in the efficient CO_2 electroreduction.

Keywords Iron porphyrin · Multiwalled carbon nanotube · CO_2 reduction

Introduction

Carbon nanotubes (CNTs) have been extensively investigated because of their fascinating nanosized structures, unique properties, and potential electronic, optical, thermal, and mechanical applications [1, 2]. Metalloporphyrin is a kind of aromatic compound with a large plane conjugated structure and a metal ion in the center, which finds many uses as homogeneous catalysts in a variety of oxidation and reduction reactions with good biocompatibility. Since porphyrin–CNT nanocomposites formed by van der Waals forces was first reported by Murakami et al. [3], many studies where porphyrin–CNT composites exhibiting good electrochemical properties have been reported [4–6]. Meanwhile, porphyrin–CNT-modified electrodes have been studied for applications in oxygen reduction [5, 6] and sensors [7–11]. It is concluded that combining the two kinds of materials in the electrode surface improves the electrochemical activity, reduces the electrode overpotential, and enables the electrodes to be further modified with bioactive substances such as enzymes. Despite these studies, the mechanism of the synergistic interaction between porphyrin and CNTs remains unclear. It is speculated that there are mutually interacting π systems in porphyrin–CNT nanohybrids [12] or that nanotubes form a conduction passage for the electron transfer reaction between the metalloporphyrin and the electrode [13]. Although light-induced electron transfer and photoinduced charge separation in porphyrin–CNT nanohybrids have been found in photoinduced processes [14, 15], however, to the best of our knowledge, little is still known of the evidence of electron transfer between metalloporphyrin and CNTs in general electrochemical processes.

As a leading cause of global warming, carbon dioxide (CO_2) is easily formed during combustion or respiration, but it is difficult to reduce. Electrochemical reduction of CO_2 has been investigated intensively as a promising approach to convert waste CO_2 to useful products [16, 17]. Catalysts containing transition metals are at the forefront of potential CO_2 electroreduction research because they feature multiple and accessible redox states that have proven to promote multiple electron transfer reactivity [18]. Metalloporphyrin was used to catalyze CO_2 electroreduction [19, 20], but

H.-Z. Zhao · Y.-Y. Chang · C. Liu
Department of Environmental Engineering,
Peking University, Beijing 100871, China

H.-Z. Zhao (✉) · Y.-Y. Chang · C. Liu
The Key Laboratory of Water and Sediment Sciences,
Ministry of Education, Beijing 100871, China
e-mail: zhaohuazhang@pku.edu.cn

electrodes modified with physically adsorbed layers of porphyrins showed poor catalytic response toward the electroreduction of CO_2 [21]. Among the porphyrin complexes studied, iron porphyrins have been demonstrated to be the most efficient homogeneous catalyst in the electrochemical reduction of CO_2 to CO [22]. Thus, iron porphyrin–CNT composites would have shown great catalytic potential for CO_2 reduction according to the excellent electrochemical activity of porphyrin–CNT composites mentioned earlier, but related study is still lacking.

In the present work, we modified glassy carbon (GC) electrodes and carbon felt (CF) electrodes with iron porphyrin and multiwalled carbon nanotubes (MWCNTs). The adsorption of iron porphyrin onto MWCNTs was characterized by scanning electron microscopy (SEM) and ultraviolet and visible spectroscopy (UV–vis). The electrochemical properties of the modified electrodes for CO_2 reduction were investigated by cyclic voltammetry (CV) and CO_2 electrolysis. The synergistic electrocatalysis mechanism was also proposed and discussed with electrochemical impedance spectroscopy (EIS) and electron paramagnetic resonance (EPR). The results shed light on the mechanism of coactions between CNTs and metalloporphyrin and will extend the scope of their applications.

Materials and methods

Chemicals and materials

MWCNTs (95 %, 10–20-nm diameter) were purchased from Shenzhen Nanotech Port Co. Ltd., People's Republic of China. Before use, MWCNTs were purified and activated with a mixture of concentrated sulfuric acid–nitric acid ($3:1 v/v$) to introduce carboxyl groups onto MWCNTs [1]. Formic dehydrogenase (FDH; Sigma Co., USA) and 5,10,15,20-tetraphenyl ferric(III) chloride porphyrin (FeTPPCl; Sigma Co., USA) were used as received. All other chemicals were of analytical grade, and all solutions were prepared with ultra-pure water obtained from a Millipore-MilliQ system with a resistivity of 18 MΩ cm. A phosphate buffer solution (PBS; 20 mM, pH 6.9) was prepared from Na_2HPO_4 (55 %) and NaH_2PO_4 (45 %) with ultra-pure water.

A GC electrode (Φ 4 mm; Tianjin Aidahengsheng Technology Co. Ltd., People's Republic of China) was polished sequentially with 1.5 μm α-Al_2O_3 and 0.5 μm α-Al_2O_3 to a mirror finish and washed with ultra-pure water in an ultrasonic bath for 3 min. A CF electrode (3.0×3.0 cm^2, Beijing Feichilvneng Co. Ltd., People's Republic of China) was washed with ultra-pure water and dried before use. The electrodes modified with GC as the substrate electrode were used for structure characterization and electrochemical behaviors, while the electrodes modified with CF as the substrate electrode were used to study the electrolysis performance.

Preparation of FeP–CNT composites

FeTPPCl was deposited electrostatically onto the carboxylated MWCNTs by stirring MWCNTs (1.0 mg) and FeTPPCl (10.0 mg) in PBS (1.0 mL, pH 6.9) at 4 °C for 12 h. Subsequently, the mixture was centrifuged thoroughly, and the mixture of FeTPPCl and MWCNTs (denoted hereafter by FeP–CNTs) was collected after carefully removing the supernatant. Final FeP–CNTs were washed with ultra-pure water to remove loosely adsorbed FeTPPCl molecules and lyophilized. UV and EPR spectroscopy were used to characterize FeP–CNTs.

Preparation of modified electrodes

FeTPPCl and MWCNTs were immobilized both individually and jointly onto the GC electrodes using the following procedure: MWCNTs were randomly deposited onto the surface of a bare GC electrode by dropping 20 μL of well-dispersed suspension of MWCNTs (0.2 mgmL^{-1} in methanol, sonicated for 1 h before use) onto the electrode surface. The electrode was subsequently dried at room temperature. The electrode without further treatment was denoted by CNT/GC hereafter. A 20 μL of FeTPPCl suspension (1.0 mgmL^{-1} in methanol, sonicated for 1 h before use) was deposited onto the GC and CNT/GC surfaces before they were dried at room temperature, which were denoted hereafter by FeP/GC and FeP–CNT/GC, respectively.

The CF electrodes modified with FeTPPCl and MWCNTs both individually and jointly were prepared with a similar procedure as follows: MWCNTs were randomly deposited onto both sides of CF by dropping 1.0 mL of well-dispersed suspension of MWCNTs (1.0 mgmL^{-1} in methanol, sonicated for 1 h before use) onto each side of the electrodes, and the electrodes were subsequently dried under an infrared lamp. The electrode without further treatment was denoted by CNT/CF hereafter. A 0.5 mL of FeTPPCl suspension (1.0 mgmL^{-1} in methanol, sonicated for 1 h before use) was deposited onto the CF and CNT/CF surfaces before they were dried at room temperature, which were denoted hereafter by FeP/CF and FeP−CNT/CF, respectively.

CO_2 electrolysis

An H-type reactor (0.5 L) shown in Scheme 1 was used as the electrolytic cell, and its electric power was supplied by a power source (DH1718E-5, Peking University Experimental Electronic Instrument Plant, China). The two compartments of the electrolytic cell were separated by a proton exchange membrane (PEM; Nafion117, 5-cm diameter, DuPont, USA).

The PEM was sequentially boiled in H_2O_2 (30 %), deionized water, an H_2SO_4 solution (0.5 M), and again in deionized water (each for 1 h) before it was immersed in deionized water for use. A bare CF electrode was used as the anode, while different modified CF electrodes, namely CF, FeP/CF, CNT/CF, and FeP–CNT/CF, were separately employed as the cathode with Ag/AgCl electrode as a reference electrode. A 0.1 M $KHCO_3$ solution was always used as the supporting electrolyte. In order to reduce CO_2 to formic acid, methyl viologen (10.0 mg, 0.20 mM), NADH (7.0 mg, 0.05 mM), and FDH (3.0 mg, 15 units L^{-1}) were added to the electrolyte. The electrolysis was performed potentiostatically by holding the cathodic potential at a certain value (−1.6 or −1.4 V) vs. Ag/AgCl reference electrode for 4 h, and the electrolyte was continuously aerated with CO_2 during the whole process. The sampling for formic acid detection was set at 1, 2, 3, and 4 h from the start of electrolysis. All potentials are given vs. Ag/AgCl electrode as the reference electrode.

Analytical methods

The surface morphology of the modified GC electrodes was investigated by SEM (NOVA NANOSEM 430, FEI), and UV–vis absorption spectra were recorded on a UV–vis–NIR spectrometer (UV 3100, Shimadzu). CV measurements were carried out in an undivided conventional three-electrode cell with 0.5 M $NaHCO_3$ electrolyte, connected to an electrochemical workstation (Par 283, USA). GC, FeP/GC, CNT/GC, and FeP–CNT/GC electrodes were each served as a working electrode. A Pt electrode (Shanghai Precision and Scientific Instrument Co. Ltd., People's Republic of China) and an Ag/AgCl electrode (sat. KCl) were chosen as the counter and reference electrodes, respectively. All potential values are in reference to Ag/AgCl unless otherwise noted, and all cyclic voltammograms were recorded in the potential range of 0 to 1,600 mV with a scan rate of 50 mV s^{-1} at ambient temperature.

Formic acid produced in the cathodic solution during the electrolysis was analyzed by ion chromatography (ICS-900 Dionex). The conditions for formic acid detection were as follows: analytical column, AS23; mobile phase, 4.5 mM Na_2CO_3/0.80 mM $NaHCO_3$; rate of flow, 1.0 mL min^{-1}; suppressor type, ASPS 4 mm; and suppressor current, 25 mA.

EIS were performed with the apparatus as used for CV in 0.2 M PBS electrolyte. FeP/GC and FeP–CNT/GC electrodes were each served as the working electrode. A frequency range of 100 kHz to 1 mHz was employed. The AC voltage amplitude used was 10 mV. The impedance diagram was presented in the form of a Nyquist plot.

EPR spectra were recorded on a Brucker EMX spectrometer. The conditions for EPR measurements were as follows: frequency, 9.6 GHz; power, 3 mW; modulation amplitude, 10 G; modulation frequency, 100 kHz; and temperature, 293 K. The environmental information of the electron was deduced from the position (described by the g value) and shape of the absorption line.

Results and discussion

Interaction between FeTPPCl and MWCNTs

SEM

As shown in the SEM images, the adsorbed MWCNTs are evenly distributed on the bare GC electrode surface (Fig. 1a), while the FeTPPCl molecules form clusters on the bare GC electrode surface, leading to uneven distribution of the modified layer (Fig. 1b). The FeTPPCl molecules are much more scattered on the MWCNT-modified GC electrode (Fig. 1c) than those on the bare electrode. FeTPPCls are tightly attached to the MWCNT-modified layer, as shown in the highly magnified image (Fig. 1d). The complicated meshwork of MWCNTs not only enlarges the adsorption surface but also wraps FeTPPCls, which favors a strong and even fixation of the FeTPPCl-modified layer.

UV–vis spectra

The UV–vis absorption spectra of FeTPPCl and FeP/CNT are presented in Fig. 2. FeP–CNTs exhibit characteristic absorption peaks at the same wavelengths as FeTPPCls, with a Soret band at 370 nm and several stronger absorptions (Q bands) at longer wavelengths (from 450 to 600 nm). It is demonstrated that the structure of FeTPPCl remains the same after being adsorbed by the MWCNTs. Compared to FeTPPCls, the absorbance of FeP–CNTs decreases markedly after their adsorption onto MWCNTs, indicating the strong adsorption of FeTPPCl onto MWCNTs [6].

CO_2 electroreduction

CV

CV was used to study the electrochemical behavior of the GC electrode modified with MWCNTs and FeTPPCl in a CO_2-saturated 0.5 M $NaHCO_3$ solution (Fig. 3). The CV curve of FeP–CNT/GC in an N_2 atmosphere was used for comparison (Fig. 3a). There are two peaks in both curves as shown in Fig. 3a: peak I corresponds to the Fe^{II}/Fe^{III} redox couple, while peak II is attributed to the oxidation of a porphyrin ring. Similar behavior was observed for iron porphyrin immobilized on SiO_2/Al_2O_3 surface [23]. Compared with the CV curve of FeP–CNT/GC in an N_2 atmosphere, an obvious positive shift in peak II is observed in the case of CO_2 reduction, and this positive shift is

Scheme 1 Schematic diagram of CO_2 electrolysis device
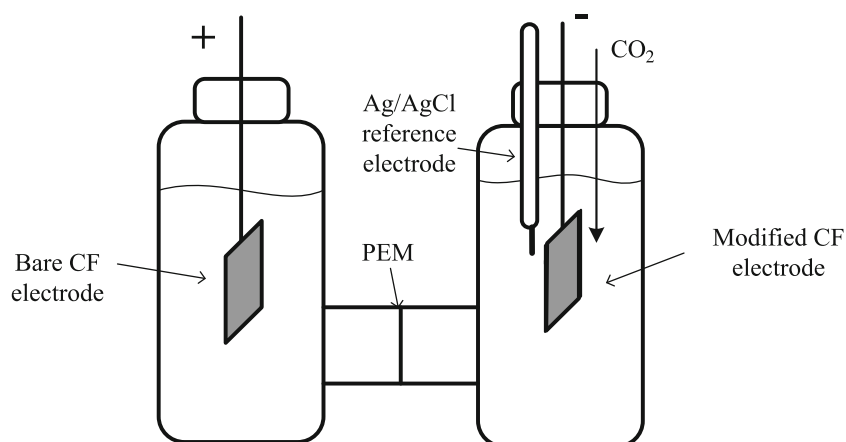
attributed to the catalytic current of CO_2 electroreduction. The results suggest that CO_2 can be catalytically electro-reduced by FeP–CNT/GC. Peak II is selected as a CO_2 reduction indicator in the following experiments.

Figure 3b presents the evolution of the cyclic voltammo-grams for GC, CNT/GC, FeP/GC, and FeP–CNT/GC in a CO_2-saturated 0.5 M $NaHCO_3$ solution. No peak corresponding to CO_2 reduction is observed on the bare GC electrode,
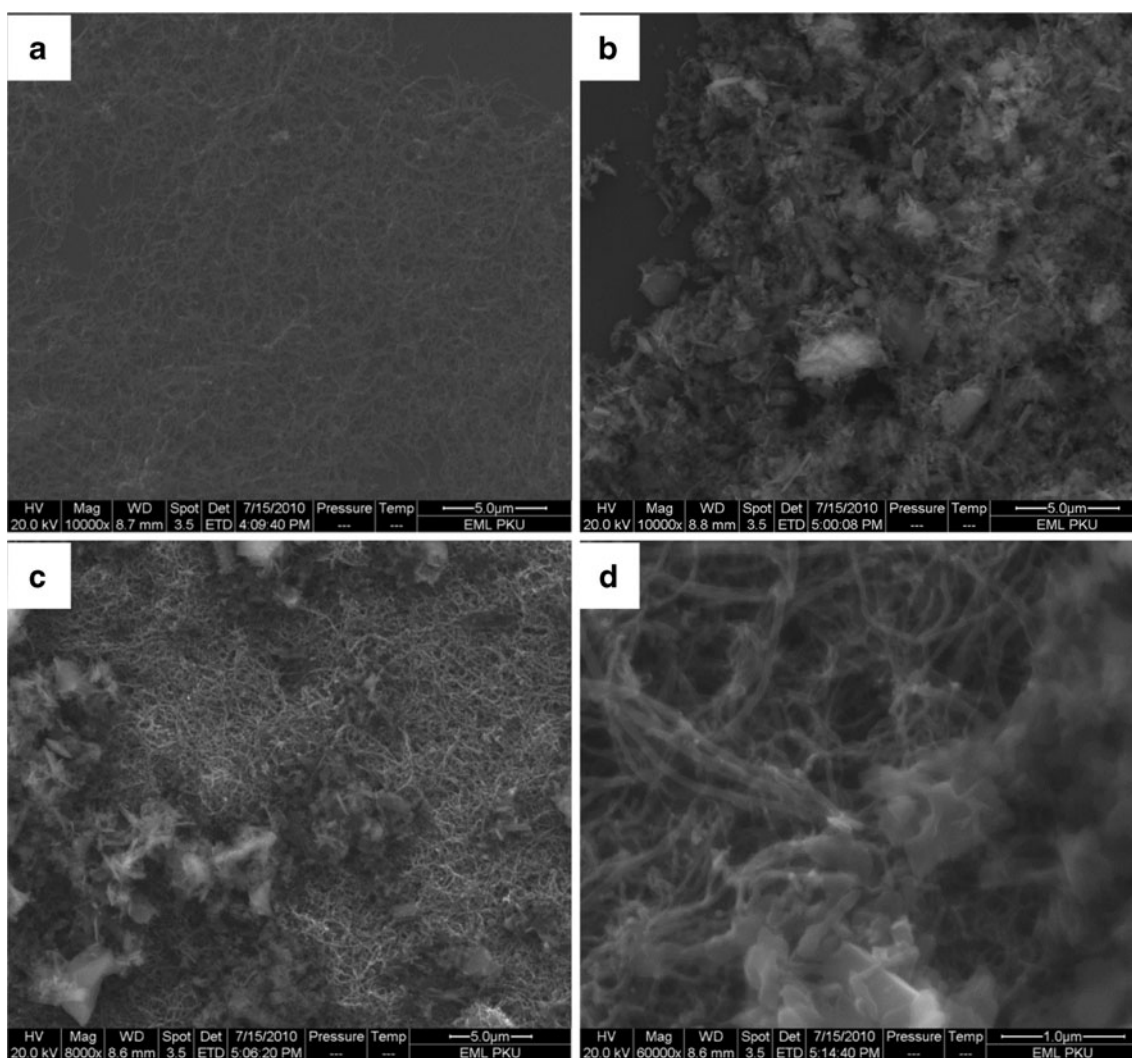
Fig. 1 SEM images of CNT/GC ($\times$10,000) (**a**), FeP/GC ($\times$10,000) (**b**), FeP–CNT/GC ($\times$8,000) (**c**), and FeP–CNT/GC ($\times$60,000) (**d**)
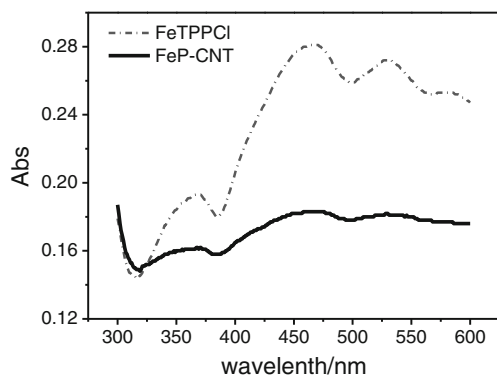
Fig. 2 UV–vis spectra of FeTPPCl before and after being adsorbed on the MWCNTs

demonstrating that the applied cathode potential is not low enough to reduce CO_2 using the GC electrode. The peak current of FeP/GC is too small to be analyzed. Combining SEM results, the small current is attributed to the uneven distribution and weak adsorption of FeTPPCl on the GC electrode. For the CNT/GC electrode, CO_2 reduction peak appears near −1.5 V. After the introduction of FeTPPCls (FeP–CNT/GC), the peak potential for CO_2 reduction is shifted positively from 0.1 to −1.4 V, and the peak current also increases markedly.
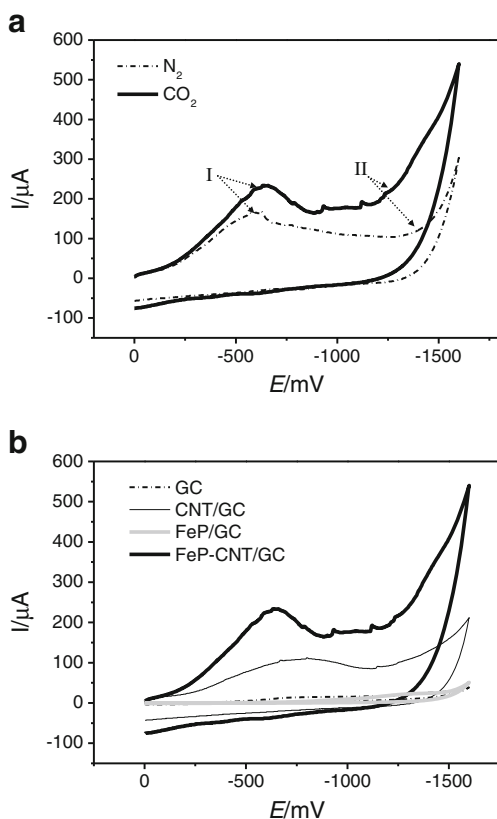

Fig. 3 Cyclic voltammograms of FeP–CNT/GC in a 0.5 M NaHCO₃ solution saturated with CO_2 and N_2 (**a**) and different modified electrodes in a 0.5 M NaHCO₃ solution saturated with CO_2 (**b**) (electrode area 0.13 cm²)

As a result, the presence of FeTPPCl prompts the electron transfer of dissolved CO_2 on the electrode surface and catalyzes its reduction, leading to a lower overpotential. Like the interaction between phthalocyanine and carbon nanotubes [24, 25], the π−π interaction between the porphyrin ring and sidewalls of MWCNTs reduces the electron density around the Fe nuclei in FeTPPCl, which expands the macrocyclic conjugated structure of FeTPPCl and further increases the potential for CO_2 reduction. The apparent surface of the modified electrode becomes larger due to the presence of FeP–CNT composite [26]. Meanwhile, the electron transfer is improved in the modified electrode films because of the excellent electrical conductivity of MWCNTs [27]. As a result, the peak current for CO_2 reduction increases markedly.

CO_2 electrolysis

Formic acid has been reported to be the only product of CO_2 reduction in the presence of FDH, NADH, and methyl viologen [28]. Similarly in the present work, only the formation of formic acid is detected by ion chromatography, and it is used to demonstrate the CO_2 electroreduction effect with different modified electrodes. According to the CO_2 reduction potential recorded by CV, the cathode potentials of the electrolysis cell are set at −1.6 and −1.4 V, and the variations in the concentration of formic acid produced at different electrolysis times at each cathode potential are showed in Fig. 4. CO_2 is successfully reduced to formic acid at all four modified electrodes when the cathode potential is set at −1.6 V (Fig. 4a). However, when the cathode potential is increased to −1.4 V, no formic acid is detected at CF and CNT/CF. In contrast, the formic acid formation at FeP–CNT/CF is only slightly influenced by the potential increase. The concentration of formic acid formed at FeP–CNT/CF is higher than that formed at the other two modified electrodes in the following order: FeP–CNT/CF> FeP/CF>CNT/CF, demonstrating that FeP–CNT/CF has higher electrocatalysis efficiency than the other two. Such efficient electrocatalysis by FeP–CNT/CF can be owed to two factors. First, the interaction between MWCNTs and FeTPPCl decreases the overpotential of reducing CO_2 to formic acid. Second, the excellent electrical conductivity of MWCNTs improved the electron transfer between CO_2 and the active sites in FeTPPCl, and thereby increasing formic acid formation. This result is in accordance with the CV results and would be further confirmed by EIS and EPR.

Mechanism of the synergistic electrocatalysis between FeTPPCl and MWCNTs

EIS

Figure 5 shows the Nyquist diagrams for FeP–CNT/GC and FeP/GC. The diagram of FeP/GC exhibits a typical shape of
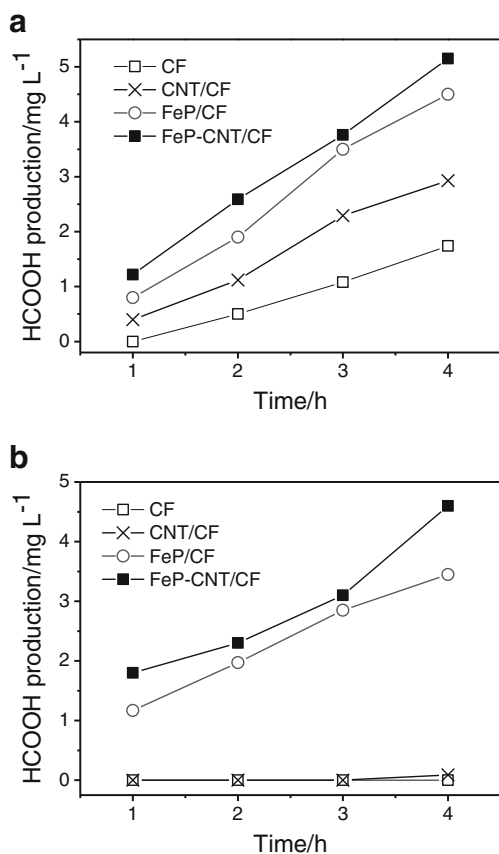
a

b

Fig. 4 Variations in the concentration of formic acid produced at different electrolysis times at the cathode potential of −1.6 V (**a**) and −1.4 V (**b**) vs. Ag/AgCl (electrode area 9 cm^2)

Scheme 2 Equivalent circuits compatible with the Nyquist diagram in Fig. 5

be presented by the Randle's equivalent circuit, as shown in Scheme 2. The total impedance is determined by several parameters [30]: the double layer capacitance (C_d) at the modified electrode–solution interface, charge transfer resistance R_{ct}, corresponding to the modified layer charge transfer process, Warburg impedance (Z_w) resulting from the diffusion of charged species from the bulk of the electrolytic solution to the interface and through the interface layer, and ohmic bulk electrolyte solution resistance (R_s).

The diameter of the semicircle corresponds to R_{ct} [8]. Here, R_{ct} of the FeP/GC cathode is estimated to be larger than 200 Ω, whereas that of the FeP–CNT/GC electrode is too low to be recorded by the EIS spectrum that exhibits a straight line at all frequencies, as shown clearly in the inset of Fig. 5. It is known that the standard heterogeneous electron transfer constant k_0 is inversely proportional to the electron transfer resistance R_{ct} [31]. Here, a prominent reduction in R_{ct} for the FeP–CNT/GC electrode is observed, which implies that the reaction rate of CO_2 reduction in the CNT-containing cathode is much faster than that in the FeP/CNT electrode, indicating higher catalytic efficiency of FeP–CNT/GC than FeP/GC.

EPR spectroscopy

As shown in Fig. 6, there is a well-defined resonance absorption centered at $g=6.41$ in the spectrum of FeTPPCl, which can be seen as an indicator for the electron spin state and coordinate state of the intrinsic FeTPPCl molecules. In the spectrum of FeP–CNT, a much weaker resonance absorption centered at $g=6.41$ is observed compared with that

electrochemical impedance, including a semicircle region lying on the Z'-axis followed by a straight line. The semicircle portion, at higher frequencies, corresponds to the electron transfer kinetics of the redox probe at the electrode interface, whereas the linear part at the lower frequency range is characteristic of diffusion-limited electron transfer processes [29]. Specifically, the complex impedance Z can
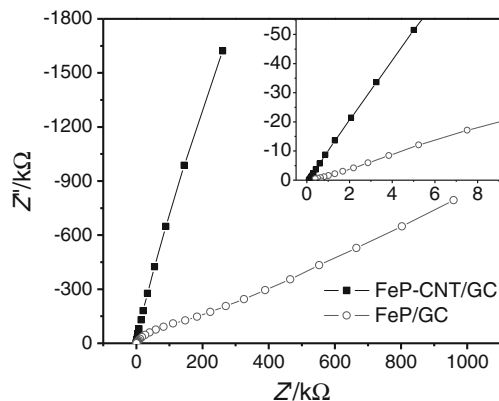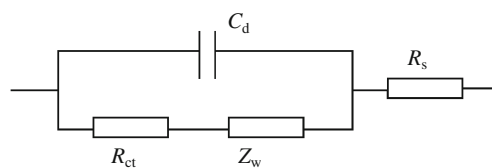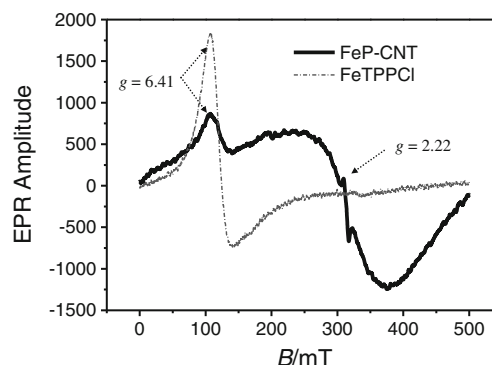

Fig. 5 Nyquist diagram of FeP/GC and FeP–CNT/GC (the *inset* represents the magnification of the high range in the Nyquist diagram)

Fig. 6 EPR spectra of ferriporphyrin before and after being adsorbed on carbon nanotubes

of FeTPPCl. Meanwhile, there are a broad resonance absorption that can be superposition of several signals, and a weak signal centered at $g=2.22$ appeared.

The resonance absorptions at $g=6.41$ in the two spectra demonstrate that part of the electrons in FeP–CNT retains the same electron spin state and coordinate state as those in FeTPPCl, and the weaker signal may be attributed to a lower spin density on the central Fe ion in FeP–CNT [32]. The newly appeared resonance absorptions for FeP–CNT are closer to that of free electron ($g=2.0023$) compared with those in FeTPPCl, indicating that part of the electrons are at higher spin states. This phenomenon is caused by two reasons. First, the interaction between MWCNTs and FeTPPCls has weakened the coupling between the electron-spin motion and molecule-orbit motion among the FeTPPCl molecules [33]. Second, some electrons at freer spin and coordinate states are introduced by the MWCNTs. X-ray structures of model compounds and proteins have shown that the high-spin iron atom is located about 0.5 Å out of the porphyrin plane, while the low-spin iron is in plane [34, 35]. Accordingly, electrons at high spin states have a relatively high energy and provide a more open microenvironment for electron transfer than low spin states. As a result, direct electron transfer between MWCNTs and FeTPPCl can be achieved and enhanced.

Conclusions

Electrodes modified with iron porphyrin and carbon nanotubes have been successfully prepared and applied to CO_2 electroreduction. The results show that iron porphyrin and CNTs can be immobilized on the surface of carbon electrodes through strong adsorption. Efficient synergistic electrocatalysis can be achieved by FeP–CNT-modified electrodes. It is demonstrated that direct electron transfer takes place between MWCNTs and iron porphyrin. Together with the increased apparent surface area and excellent electrical conductivity of MWCNTs, the electrode interface resistance greatly decreases. As a result, the overpotential for CO_2 reduction decreases and the reaction rate increases. The results demonstrate the great potential for iron porphyrin–CNT-modified electrodes in the efficient and energy-saving CO_2 electroreduction.

References

1. Sun JJ, Zhao HZ, Yang QZ, Song J, Xue A (2010) A novel layer-by-layer self-assembled carbon nanotube-based anode: preparation, characterization, and application in microbial fuel cell. Electrochim Acta 55(9):3041–3047

2. Qiao Y, Li CM (2011) Nanostructured catalysts in fuel cells. J Mater Chem 21(12):4027–4036

3. Murakami H, Nomura T, Nakashima N (2003) Noncovalent porphyrin-functionalized single-walled carbon nanotubes in solution and the formation of porphyrin-nanotube nanocomposites. Chem Phys Lett 378(5–6):481–485

4. Zhao Q, Gu ZN, Zhuang QK (2004) Electrochemical study of tetra-phenyl-porphyrin on the SWNTs film modified glassy carbon electrode. Electrochem Commun 6(1):83–86

5. Kowalewska B, Skunik M, Karnicka K, Miecmikowski K, Chojak M, Ginalska G, Belcarz A, Kulesza PJ (2008) Enhancement of bio-electrocatalytic oxygen reduction at the composite film of cobalt porphyrin immobilized within the carbon nanotube-supported peroxidase enzyme. Electrochim Acta 53(5):2408–2415

6. Choi A, Jeong H, Kim S, Jo S, Jeon S (2008) Electrocatalytic reduction of dioxygen by cobalt porphyrin-modified glassy carbon electrode with single-walled carbon nanotubes and nafion in aqueous solutions. Electrochim Acta 53(5):2579–2584

7. Liu Y, Yan YL, Lei HP, Wu F, Ju HX (2007) Functional multi-walled carbon nanotube nanocomposite with iron picket-fence porphyrin and its electrocatalytic behavior. Electrochem Commun 9(10):2564–2570

8. Ma QA, Ai SY, Yin HS, Chen QP, Tang TT (2010) Towards the conception of an amperometric sensor of L-tyrosine based on Hemin/PAMAM/MWCNT modified glassy carbon electrode. Electrochim Acta 55(22):6687–6694

9. Penza M, Rossi R, Alvisi M, Valerini D, Serra E, Paolesse R, Martinelli E, D'Amico A, Di Natale C (2011) Metalloporphyrin-modified carbon nanotube layers for gas microsensors. Sens Lett 9(2):913–919

10. Luz RCS, Damos FS, Tanaka AA, Kubota LT, Gushikem Y (2008) Electrocatalysis of reduced L-glutathione oxidation by iron(III) tetra-(N-methyl-4-pyridyl)-porphyrin (FeT4MPyP) adsorbed on multi-walled carbon nanotubes. Talanta 76(5):1097–1104

11. Chen W, Ding Y, Akhigbe J, Bruckner C, Li CM, Lei Y (2010) Enhanced electrochemical oxygen reduction-based glucose sensing using glucose oxidase on nanodendritic poly[meso-tetrakis(2-thienyl)porphyrinato]cobalt(II)-SWNTs composite electrodes. Biosens Bioelectron 26(2):504–510

12. Rahman GMA, Guldi DM, Campidelli S, Prato M (2006) Electronically interacting single wall carbon nanotube-porphyrin nanohybrids. J Mater Chem 16(1):62–65

13. Murakami H, Nakamura G, Nomura T, Miyamoto T, Nakashima N (2007) Noncovalent porphyrin-functionalized single-walled carbon nanotubes: solubilization and spectral behaviors. J Porphyrins Phthalocyanines 11(5–6):418–427

14. Chitta R, Sandanayaka ASD, Schumacher AL, D'Souza L, Araki Y, Ito O, D'Souza F (2007) Donor-acceptor nanohybrids of zinc naphthalocyanine or zinc porphyrin noncovalently linked to single-wall carbon nanotubes for photoinduced electron transfer. J Phys Chem C 111(19):6947–6955

15. Hasobe T, Murata H, Kamat PV (2007) Photoelectrochemistry of stacked-cup carbon nanotube films. Tube-length dependence and charge transfer with excited porphyrin. J Phys Chem C 111(44):16626–16634

16. Benson EE, Kubiak CP, Sathrum AJ, Smieja JM (2009) Electrocatalytic and homogeneous approaches to conversion of CO_2 to liquid fuels. Chem Soc Rev 38(1):89–99

17. Oloman C, Li H (2008) Electrochemical processing of carbon dioxide. Chemsuschem 1(5):385–391

18. Morris AJ, Meyer GJ, Fujita E (2009) Molecular approaches to the photocatalytic reduction of carbon dioxide for solar fuels. Acc Chem Res 42(12):1983–1994

19. Behar D, Dhanasekaran T, Neta P, Hosten CM, Ejeh D, Hambright P, Fujita E (1998) Cobalt porphyrin catalyzed reduction of CO_2. Radiation chemical, photochemical, and electrochemical studies. J Phys Chem A 102(17):2870–2877

20. Magdesieva TV, Yamamoto T, Tryk DA, Fujishima A (2002) Electrochemical reduction of CO_2 with transition metal phthalocyanine and porphyrin complexes supported on activated carbon fibers. J Electrochem Soc 149(6):D89–D95

21. Ramirez G, Lucero M, Riquelme A, Villagran M, Costamagna J, Trollund E, Aguirre MJ (2004) A supramolecular cobalt-porphyrin-modified electrode, toward the electroreduction of CO_2. J Coord Chem 57(3):249–255

22. Bhugun I, Lexa D, Savéant JM (1996) Catalysis of the electrochemical reduction of carbon dioxide by iron(0) porphyrins. Synergistic effect of Lewis acid cations. J Phys Chem 100(51):19981–19985

23. Fujiwara ST, Gushikem Y, Pessoa CA, Nakagaki S (2005) Electrochemical studies of a new iron porphyrin entrapped in a propylpyridiniumsilsesquioxane polymer immobilized on a SiO_2/Al_2O_3 surface. Electroanalysis 17(9):783–788

24. Yang YB, Xu L, Li FY, Du XG, Sun ZX (2010) Enhanced photovoltaic response by incorporating polyoxometalate into a phthalocyanine-sensitized electrode. J Mater Chem 20(48):10835–10840

25. Mamuru SA, Ozoemena KI, Fukuda T, Kobayashi N, Nyokong T (2010) Studies on the heterogeneous electron transport and oxygen reduction reaction at metal (Co, Fe) octabutylsulphonylphthalocyanines supported on multi-walled carbon nanotube modified graphite electrode. Electrochim Acta 55(22):6367–6375

26. Liu XQ, Feng HQ, Liu XH, Wong DKY (2011) Electrocatalytic detection of phenolic estrogenic compounds at NiTPPS vertical bar carbon nanotube composite electrodes. Anal Chim Acta 689(2):212–218

27. Zhao HZ, Zhang Y, Zhao B, Chang YY, Li ZS (2012) Electrochemical Reduction of carbon dioxide in an MFC-MEC system with a layer-by-layer self-assembly carbon nanotube/cobalt phthalocyanine modified electrode. Environ Sci Technol 46(9):5198–5204

28. Reda T, Plugge CM, Abram NJ, Hirst J (2008) Reversible inter-conversion of carbon dioxide and formate by an electroactive enzyme. Proc Natl Acad Sci USA 105(31):10654–10658

29. Lu XQ, Zhi FP, Shang H, Wang XY, Xue ZH (2010) Investigation of the electrochemical behavior of multilayers film assembled porphyrin/gold nanoparticles on gold electrode. Electrochim Acta 55(11):3634–3642

30. Li XF, Wan Y, Sun CQ (2004) Covalent modification of a glassy carbon surface by electrochemical oxidation of r-aminobenzene sulfonic acid in aqueous solution. J Electroanal Chem 569(1):79–87

31. Xiao F, Liu LQ, Li J, Zeng JJ, Zeng BZ (2008) Electrocatalytic oxidation and voltammetric determination of nitrite on hydrophobic ionic liquid-carbon nanotube gel-chitosan composite modified electrodes. Electroanalysis 20(18):2047–2054

32. Cambré S, Wenseleers W, Goovaerts E, Resasco DE (2010) Determination of the metallic/semiconducting ratio in bulk single-wall carbon nanotube samples by cobalt porphyrin probe electron paramagnetic resonance spectroscopy. ACS Nano 4(11):6717–6724

33. Elliott RJ (1954) Theory of the effect of spin-orbit coupling on magnetic resonance in some semiconductors. Phys Rev 96(2):266–279

34. Perutz MF (1970) Stereochemistry of cooperative effects in haemoglobin. Nature 228(5273):726–734

35. Hoard JL (1971) Stereochemistry of hemes and other metalloporphyrins. Science 174(4016):1295–1302